*Progress In Electromagnetics Research B, Vol. 16, 229–245, 2009*

# DESIGN OF A WIDE-ANGLE BICONICAL ANTENNA FOR WIDEBAND COMMUNICATIONS

**D. Ghosh and T. K. Sarkar**

Department of Electrical Engineering and Computer Science
Syracuse University
Syracuse, NY 13244, USA

**E. L. Mokole**

Radar Division, Naval Research Laboratory
Washington, DC 20375, USA

**Abstract**—The wide-angle bicone antenna terminated by a spherical cap is investigated. The antenna radiation patterns have been observed for various values of $ka$ where $k$ represents the phase constant and $a$ represents the conical length. It is seen that for large values of $ka$ the radiation pattern is limited within an angular sector bounded by the cones of the antenna. Next the antenna is optimized for ultra-wideband (UWB) operation through the use of loading techniques. The transient wideband radiated and received responses of the antenna have been observed and the relationship between the wave shapes of the transient field and the input pulse have been determined.

## 1. INTRODUCTION

This paper analyzes the wide angle biconical antenna terminated by a truncated spherical cap. The antenna is suitable for operation over a wide band of frequencies. Wideband operation is possible because the truncated spherical cap reduces the reflections from the antenna structure by preventing the sudden termination of the cones. The biconical antenna has been previously analyzed by Schelkunoff [1], Smith [2], Papas and King [3, 4], and more recently by Sandler and King [5] and Samaddar and Mokole [6]. Various exact and approximate analytical expressions for the driving impedance, the effective height and the radiated field of the bicone have been derived in Refs. [1–6].

Corresponding author: D. Ghosh (deghosh@gmail.com).

In this paper the biconical antenna has been modeled and simulated in frequency domain using a program that utilizes the Electric Field Integral Equation (EFIE) to evaluate the currents on the structures [7]. The numerical results have been compared to the theoretically derived radiation fields in Section 3 of this paper. The radiation patterns have been studied to determine the effect of the variation of the cone angles of the antenna.

In addition to the radiation patterns, the transient radiation and reception from the bicone antenna have been obtained. The time-domain data is derived via the inverse Fourier transform of the frequency domain data using the Fast-Fourier-Transform (FFT) technique. The FFT process imposes certain limits on the time domain data. In particular, the time domain response becomes periodic and the total time span of the response is controlled by the lowest frequency of operation. The proper choice of frequency bands and frequency spacing for the computation makes this transformation procedure very helpful as will be shown in this paper. The relationship between the input voltages and the radiated or the received fields have been obtained for both electrically large and electrically small antennas. In order to use the biconical antenna in UWB communications, a traveling-wave bicone is obtained by reducing the reflections from the antenna structures. To a certain degree, this can be accomplished by properly designing the antenna, as done in this case by using a spherical cap on the cones. Additionally, loading with a predetermined resistive

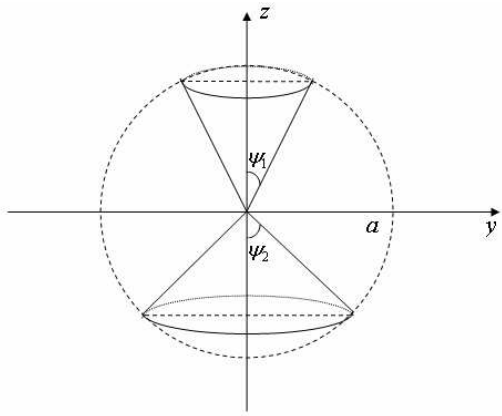


**Figure 1.** Model of spherically-capped biconical antenna. [$a$ represents the length of the cone, $\psi_1$ and $\psi_2$ represent the half cone angles of the bicone].

profile reduces the dispersion from the antenna to a great degree. This approach will be discussed in Section 4 of this paper.

## 2. ANTENNA STRUCTURE

The antenna structure is shown in Figure 1. It is axially symmetric and it has wide cone angles with the half cone angle exceeding 40°. The half cone angles are $\psi_1$ and $\psi_2$, and they satisfy $0 < \psi_1 < \pi/2$ and $0 < \psi_2 \leq \pi - \psi_1$. The cones are excited symmetrically at the apices. Three different configurations are considered in the following analysis: 1) $\psi_1 = 53.1^\circ = \psi_2$, 2) $\psi_1 = 53.1^\circ$ and $\psi_2 = 70^\circ$ and 3) $\psi_1 = 53.1^\circ$ and $\psi_2 = 90^\circ$. Case 1 represents a bicone antenna with equal cone angles whereas cases 2 and 3 are bicones with unequal cone angles. Case 3 is a special case of bicone antenna commonly referred to as the discone antenna.

## 3. RADIATION PATTERNS OF THE ANTENNA

### 3.1. With Equal Cone Angles

A bicone with cone angles of $\psi_1 = 53.1^\circ = \psi_2$ is shown in Figure 2. The conical length is $a = 0.056\,\text{m}$. The feed wire located between the tips of the two cones has a length of 4 mm and a radius of 0.1 mm. The antenna is excited symmetrically through the feed wire. Due to the presence of equal cone angles, it suffices to illustrate the upper half of the radiation pattern only. Moreover due to azimuthal symmetry the pattern can be represented in two dimensions only, the third dimension providing no extra information in this case.

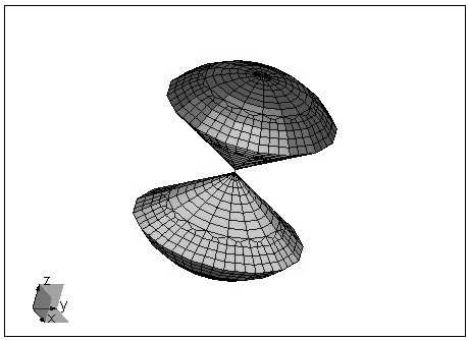


**Figure 2.** Structure of the equal angle biconical antenna.

The radiation pattern of the antenna is shown in Figure 3 for different values of $ka$ where $k$ is the phase constant. In Figure 3 the bold dotted line represents the angular value of $\psi_1 = 53.1°$, the angle being measured from the vertical axis of the structure. For representing electrically small structures with $ka \ll 1$, a value of $ka = 0.0106$ has been chosen and the corresponding radiation pattern is shown in Figure 3(a). The radiation pattern in Figure 3(a) is a close approximation to the $\sin\theta$ pattern observed for electrically small dipoles. This means that the electrically small bicone antenna has a radiation pattern similar to that of a short dipole. It is seen from Figure 3(b) that for $ka \sim 1$ the pattern is identical to that for $ka \ll 1$. So the electrically small structure approximation is valid till $ka \sim 1$.

For an electrically larger structure, the pattern breaks down into a number of smaller lobes progressively as the value $ka$ increases as seen in Figures 3(c)–3(f). In Figure 3(e) it is seen that the pattern maximum occurs at an angle of about 25° from the broadside direction. The case of an electrically large bicone with $ka \gg 1$ is approximated by $ka = 106.395$ and the radiation pattern at this value is shown in Figure 3(f). In this case the pattern maximum occurs in the

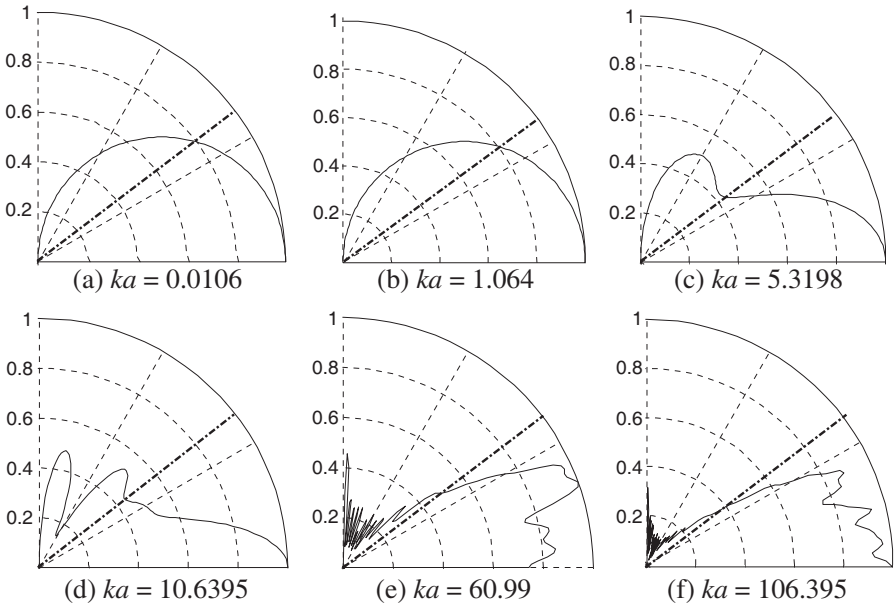


**Figure 3.** The normalized $E$-plane radiation pattern for different values of $ka$ for an equal angle bicone antenna.

broadside direction. Moreover, for both Figure 3(e) and Figure 3(f) the radiation pattern lies within 36.9° of the broadside direction where $(\pi/2 - \psi_1) = 36.9°$ represents the conical angle defined by the bicone structure. These patterns show that for electrically large bicone antennas most of the energy is concentrated in the conical area outlined by the conical edges and when $ka$ is sufficiently large, the pattern has a maximum in the broadside direction with very little energy radiating outside the above mentioned area. Thus if the directivity requirements of the communication system under consideration are known, one can design a biconical antenna to suit the application by determining the cone angles of the antenna. While designing such an antenna, it is important to remember that the designed antenna has to be used in a frequency range limited by $ka \gg 1$.

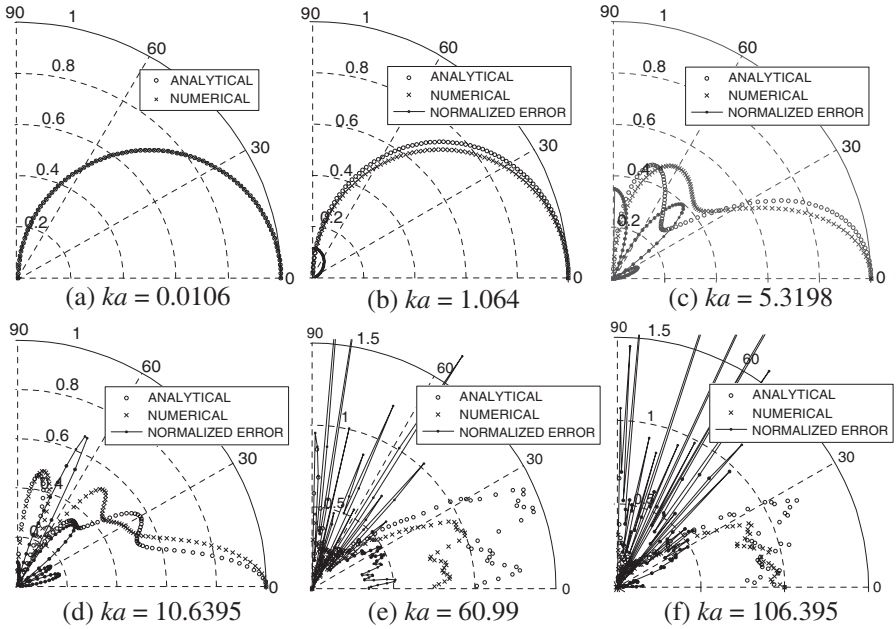


**Figure 4.** Comparison of the normalized $E$-plane radiation patterns and the error for an equal angle bicone antenna.

### 3.2. Comparison of the Radiation Patterns Obtained from Analytical and Numerical Calculations

The relative radiated field pattern in the $E$-plane can be calculated analytically as follows [4]:

$$R(\theta,\omega) = \frac{E_\theta^{rad}(r,\theta,\omega)}{E_\theta^{rad}(r,\pi/2,\omega)} = \frac{\sum_{n=1}^{\infty} \frac{i^{n-1}(2n+1)}{2n(n+1)} \frac{P^1(\cos\theta) g_n(\mu_1,\mu_2)}{h_{n-1}^{(2)}(ka) - \frac{n}{ka} h_n^{(2)}(ka)}}{\sum_{n=1}^{\infty} \frac{i^{n-1}(2n+1)}{2n(n+1)} \frac{P^1(0) g_n(\mu_1,\mu_2)}{h_{n-1}^{(2)}(ka) - \frac{n}{ka} h_n^{(2)}(ka)}} \quad (1)$$

Each series in (1) is truncated after $(M+1)$ terms where $M$ is given in the Table 1 of [6]. The analytically calculated radiated field is compared to the field obtained numerically as described in the previous section. The comparison shows that as the value of $ka$ increases the difference in the two calculations is larger. The normalized error between the theoretical and numerical results is calculated as $\frac{\|R_{theo} - R_{num}\|}{\|R_{theo}\|}$, where $R_{theo}$ in the theoretical field and $R_{num}$ is the numerically calculated field and they are shown in Figures 4(a)–4(f). When $ka \leq 10.6395$ the fields are identical differing slightly between 35° and 70°. But for $ka > 10.6395$ the difference between the theoretical and numerical calculations is much more significant due to the approximations in the theoretical calculation.

### 3.3. With Unequal Cone Angles

*3.3.1. Cone Angles of $\psi_1 = 53.1°$ and $\psi_2 = 70°$*

A bicone with $\psi_1 = 53.1°$ and $\psi_2 = 70°$ and a cone length of $a = 0.056$ m is shown in Figure 5. The antenna has a feed wire of length 4 mm and radius 0.1 mm connecting the tips of the two cones and it is excited symmetrically through the feed wire. Due to azimuthal

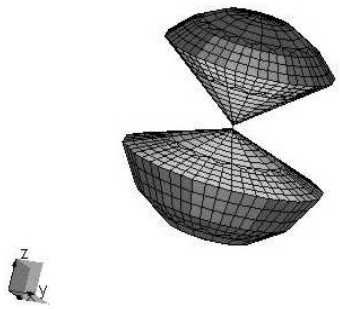


**Figure 5.** Structure of the unequal angle biconical antenna.

symmetry of the structure a two dimensional pattern is sufficient for observation purposes.

The radiation patterns of the antenna for different values of $ka$ are shown in Figure 6. In Figure 6 the dotted line in the upper plane represents the angular value of $\psi_1 = 53.1^\circ$ whereas the dotted line in the lower plane represents the angular value of $\psi_2 = 70^\circ$, the angles being measured from the vertical axes of the structure shown in Figure 1. In the case of an electrically small structure where $ka \ll 1$ the pattern is similar to that of a short dipole antenna approximated by $\sin\theta$ as shown in Figure 6(a). Figures 6(b)–6(d) show the radiation

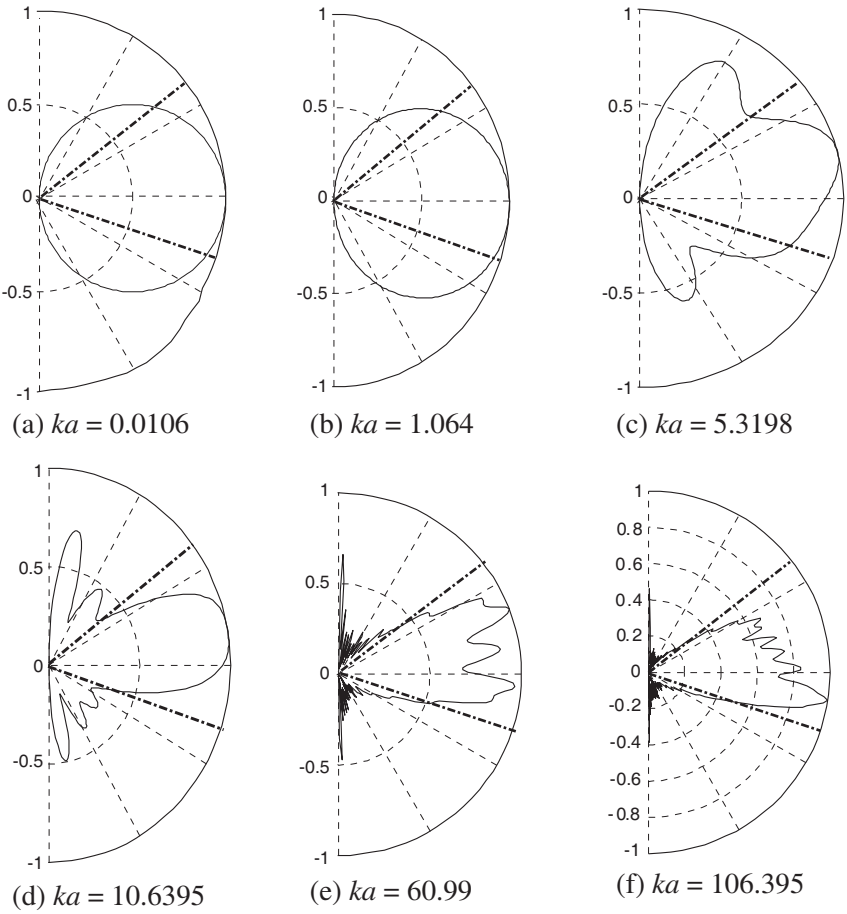


**Figure 6.** The normalized $E$-plane radiation pattern for different values of $ka$ for an unequal angle bicone antenna.

patterns of the antenna for three transitional values of $ka$. The case of electrically large bicone where $ka \gg 1$ is approximated by $ka = 60.99$ in Figure 6(e) and by $ka = 106.395$ in Figure 6(f). In Figures 6(e) and 6(f) the patterns break down into a number of small lobes. For both Figure 6(e) and Figure 6(f) the radiation pattern lies within an angular area limited by 36.9° above and 20° below the broadside direction where $(\pi/2 - \psi_1) = 36.9°$ and $(\pi/2 - \psi_2) = 20°$. These calculations verify that for electrically large biconical structures most of the energy is concentrated in the conical area outlined by the cone angles of the bicone. During the design of a communication or radar system, one can determine the angles between which the radiation has to be limited for the specific application at hand. Then using the angular data obtained, a biconical antenna can be designed to suit the application.

*3.3.2. Cone Angles of* $\psi_1 = 53.1°$ *and* $\psi_2 = 90°$

A bicone with $\psi_1 = 53.1°$ and $\psi_2 = 90°$ and a cone length of $a = 0.056\,\text{m}$ is shown in Figure 7. This is a special case of unequal cone angles of the spherically-capped bicone antenna as this antenna is similar to a discone antenna with spherical caps. Like the previous cases the antenna has a feed wire of length 4 mm and radius 0.1 mm connecting the tips of the two cones. The antenna is excited symmetrically through the feed wire. Due to azimuthal symmetry of the structure a two dimensional radiation pattern is shown.

The radiation pattern of the antenna for different values of $ka$ is shown in Figure 8. Two dotted lines are drawn in Figure 8, one represents the angular value of $\psi_1 = 53.1°$ and the other represents $\psi_2 = 90°$, the angles being measured from the vertical axis of the structure shown in Figure 1. In the case of an electrically small structure where $ka \ll 1$ the pattern is similar to that of a short dipole

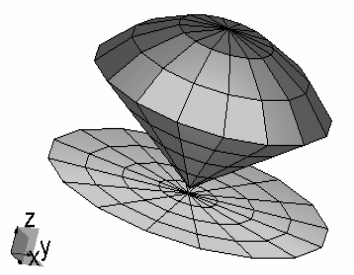


**Figure 7.** Structure of the spherically-capped discone antenna.

pattern approximated by $\sin\theta$ as shown in Figures 8(a) and 8(b). It is important to note that in these cases the pattern in not bounded by conical edges on the antenna. Observation of Figures 8(c)–8(f) progressively shows that as $ka$ increases the radiation pattern is more and more limited within the angular area determined by the two dotted lines. Again, these calculations verify that for $ka \gg 1$ the antenna radiates within a specified angular region with negligible radiation outside the area defined the cone angles on the antenna. All the radiated energy is concentrated in the upper half of the plane as shown in Figures 8(e) and 8(f).

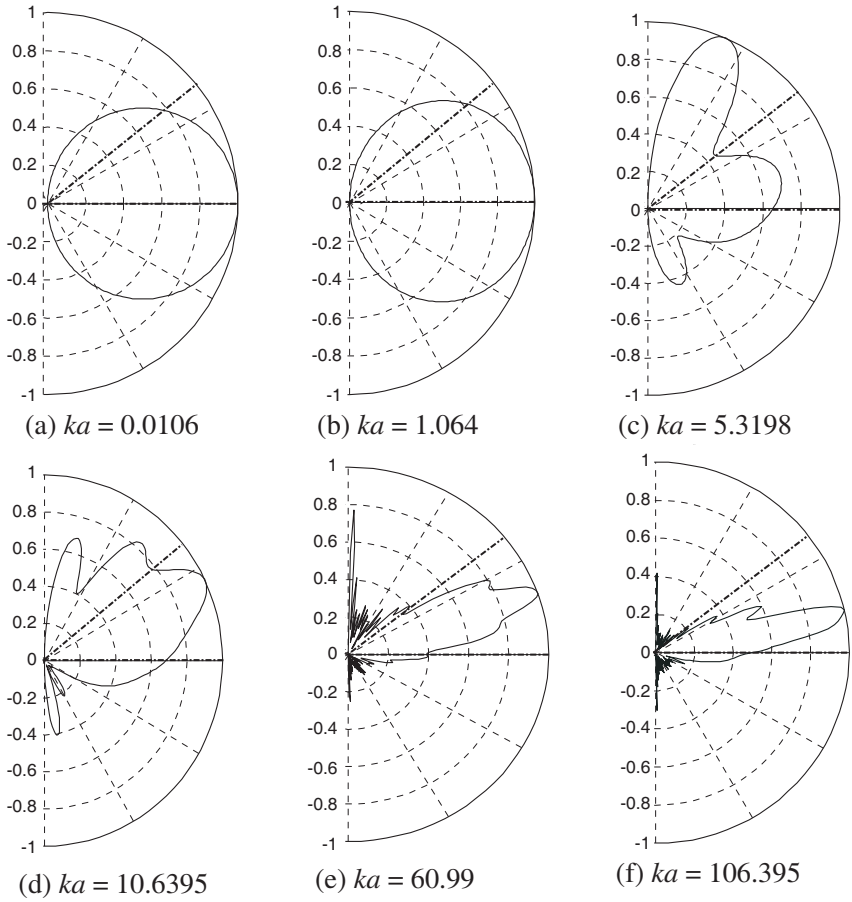


**Figure 8.** The normalized $E$-plane radiation pattern for different values of $ka$ for a spherically-capped discone antenna.

## 4. TRANSIENT RADIATED AND RECEIVED FIELDS OF A BICONE

In Section 3, it is shown that depending on the requirements of the system, a biconical antenna can be designed to have a radiation pattern directed in a desired region. This is an important step in efficient system design. Additionally, many of the current communication and radar systems call for wideband antennas. Thus it is very useful to design a bicone antenna which is directive as well as wideband. This section will address the design of ultra-wideband or UWB bicone antennas. Again in the previous section, it is shown that an electrically small bicone antenna behaves very similarly to a dipole antenna both demonstrating isotropic patterns. But the difference is that the dipole is a very narrowband antenna whereas the spherically capped bicone antenna has much wider bandwidth. Thus if the communication system warrants an antenna with a dipole-like wideband pattern, then the wideband biconical antenna can be used for such applications. Before illustrating the design of a wideband bicone structures, the commonly used wideband input pulses are investigated.

### 4.1. Input Pulse

Commonly used baseband pulses are impulses and monocycles. The monocycle is a doublet formed by the differentiation of the impulse or by the double-differentiation of the step function. As the monocycle has both positive and negative pulses, it is useful for driving both halves of the symmetrical biconical antennas. Additionally, the symmetrical nature of the monocycle does not permit the generation of dc currents during numerical computation, so the output of an antenna excited by a monocycle pulse has no dc component. The usefulness of the monocycle pulse is evident from the paper by Ghosh, et al. [8] where the monocycle has been successfully used as input to various UWB antennas. In this case, the monocycle pulse is obtained by taking the time derivative of a short duration Gaussian pulse. The monocycle pulse has the form

$$\vec{E}^{inc}(t) = \vec{u}_i \, \frac{E_0}{\sigma\sqrt{\pi}} \, \frac{d}{dt} \left\{ \exp\left( -\frac{\left(t - t_0 - \vec{r}\cdot\vec{k}\right)^2}{\sigma^2} \right) \right\} \tag{2}$$

where $\vec{u}_i$ is the unit vector that defines the polarization of the incoming plane wave, $E_0$ is the amplitude of the incoming wave (chosen to be $377\,\mathrm{V/m}$), $\sigma$ controls the width of the pulse, $t_0$ is the delay that is used

to ensure the pulse rises smoothly from 0 at the initial time to its value at time $t$, $\vec{r}$ is the position of an arbitrary point in space, and $\vec{k}$ is the unit wave vector defining the direction of arrival of the incident pulse. The frequency spectrum of (2) is given by

$$E(j\omega) = \vec{u}_i E_0 j\omega \exp\left(-\frac{\sigma^2\omega^2}{4} - j\omega\left(t_0 + \vec{r}\cdot\vec{k}\right)\right) \tag{3}$$

where $f$ is the frequency of the signal and $\omega = 2\pi f$.

The duration of the pulse is chosen corresponding to the frequency range of operation of the antenna. In the case of an electrically small bicone antenna, simulation is done between 3 MHz and 300 MHz. The input monocycle has a width of 4.5 lm and a time delay of 9 lm. Throughout the paper the unit of time is a light meter (lm), a measure of the time required by light to travel 1 m. So 1 lm = (speed of light)$^{-1}$ = $3.3333 \times 10^{-9}$ s. The input pulse is shown in Figure 9(a). For an electrically large bicone antenna, simulation is carried out for a wide band of frequencies ranging from 300 MHz to 26 GHz. The input pulse has a width of 0.0437 lm and a time delay of 0.0575 lm. This input pulse is shown in Figure 9(b). The transient fields are normalized for comparison purposes.

### 4.2. Electrically Small Antenna with Dipole-like Radiation Pattern

The transient radiated and received fields of the antenna for the three different cases discussed above are obtained. The cases are: case 1:

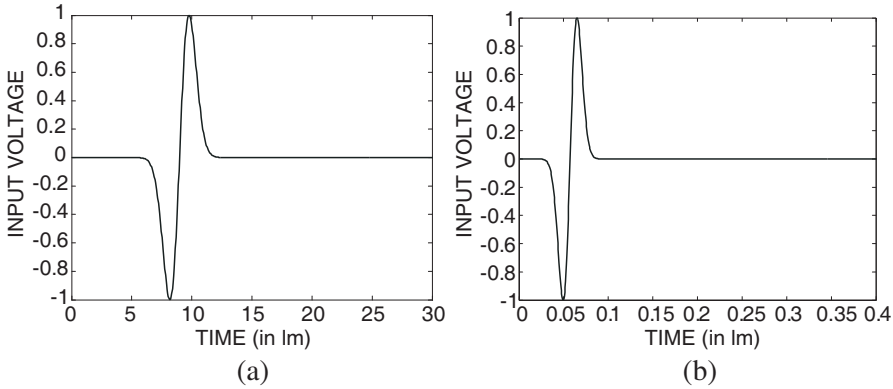


**Figure 9.** (a) Monocycle input pulse for electrically small antenna. (b) Monocycle input pulse for electrically large antenna.

$\psi_1 = 53.1^\circ = \psi_2$, case 2: $\psi_1 = 53.1^\circ$ and $\psi_2 = 70^\circ$, and case 3: $\psi_1 = 53.1^\circ$ and $\psi_2 = 90^\circ$. In each case, the antenna is simulated as a radiator and the radiated field is observed in the broadside direction. Next the antenna is simulated as a receiver for an incident wave approaching from the broadside direction. The simulation is done over a frequency range of 3 MHz to 300 MHz such that $ka < 1.064$ and the transient fields are obtained by the procedure explained in Section 1 of this paper. It has been shown in Section 3 that for values of $ka < 1.064$, the antenna behaves as an electrically small structure. The radiated fields due to the input pulse of Figure 9(a) for all the three cases are shown in Figure 10(a) and the induced currents on the bicones for an incident wave as in Figure 9(a) are shown in Figure 10(b). Figure 10 shows that the transient responses of all the three antennas are exactly same, signifying that the change in cone angle has no effect on the transient response of the antenna if the antenna is operated in the range of $ka \ll 1$.

As the antenna has a pattern similar to that of a short dipole as shown in Figures 3(a), 6(a) and 8(a), the radiated field of the bicone should be similar to the radiated field of a short dipole. In the case of an electrically small dipole, the far field is proportional to the second temporal derivative of the transient current on the structure whereas the received open circuit voltage is approximately the derivative of the incident field [8, 9]. This statement is verified by Figure 10(a) where the radiated field is the second derivative of the monocycle input voltage shown in Figure 9(a) and by Figure 10(b) where the received field is the derivative of the monocycle incident wave of Figure 9(a). As the radiated and received fields do not show any ringing, this antenna is suitable for ultra-wideband application for $ka \ll 1$.

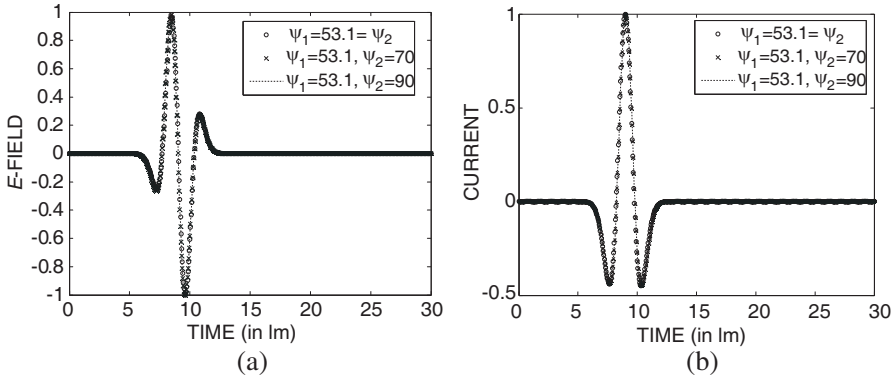


**Figure 10.** Radiated field for an electrically small antenna.

### 4.3. Electrically Large Antenna for Angle-specific Applications

Next the antenna is simulated over a very wide band of frequencies ranging from 300 MHz to 26 GHz, such that the antenna is suitable for ultra wideband operation. The input pulses used are shown in Figure 9. The radiated fields are shown in Figure 11(a) for all three cases of cone angles and when the bicones are used as receivers the induced currents are shown in Figure 11(b). The radiated field of an electrically large biconical antenna is very similar to that of a long dipole antenna. In the case of an infinitely long dipole antenna, the transmit transfer function is almost flat with respect to frequency [10]. So if the antenna is an approximation to an infinitely long antenna, the radiated field should be a close replica of the driving point voltage. Again Kanda has shown that the transmitting transient response is proportional to the time derivative of the receiving transient response [11]. So, it follows that the induced current will be an integral of the incident field. These statements are verified by Figure 11(a) where the radiated field is a close replica of the monocycle input voltage and by Figure 11(b) where the received field is an integral of the monocycle incident wave.

But the radiated field also contains reflections due to finite nature of the antenna as evident by the presence of a reflected pulse at around 0.26 lm in Figure 11. It should be noted that as the conical length of the antenna is 0.056 m, the reflected pulse should arrive after approximately $(2 \times 2 \times 0.056) = 0.224$ lm after the input pulse which has a delay of 0.0575 lm. From Figure 11 one can conclude that the transient fields differ slightly for the different values of cone angles. In particular, it is seen that the discone antenna with $\psi_2 = 90^\circ$ has larger reflection than the other cases during both radiation and reception.

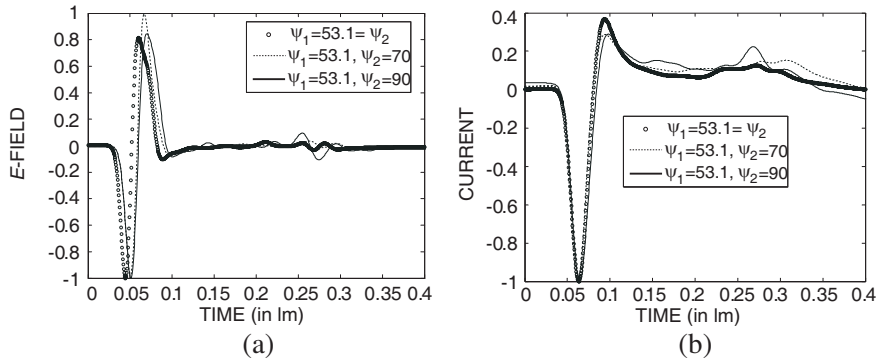


(a) (b)

**Figure 11.** Radiated field for an electrically large antenna.

In many UWB applications, it is desired that the antennas radiate most of the energy along the direction where the pulse is most similar to the exciting waveform or its derivative. For achieving this we need to reduce the dispersion from the antennas. Loading the antenna with a predetermined resistive profile reduces the dispersion from the antenna. Application of the loading profile has been illustrated for different antennas in [8]. If the antenna has a height of $2h$ and a radius of $r$, the parameter $\psi$ used for obtaining the loading profile [8] can be defined as follows:

$$\psi = 2\left[\sinh^{-1}\frac{h}{r} - C(2kr, 2kh) - jS(2kr, 2kh)\right] + \frac{j}{kh}\left(1 - e^{-j2kh}\right) \quad (4)$$

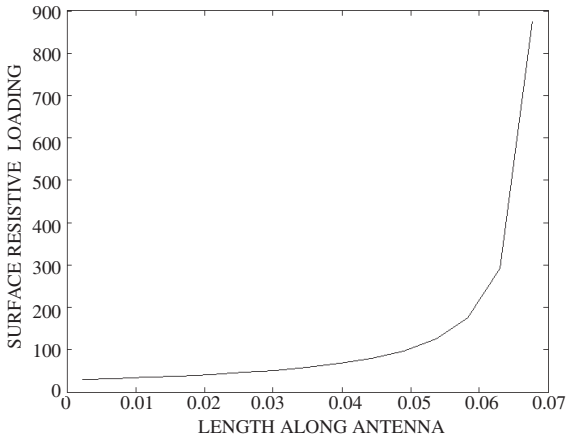


**Figure 12.** The resistive loading profile along the antenna.

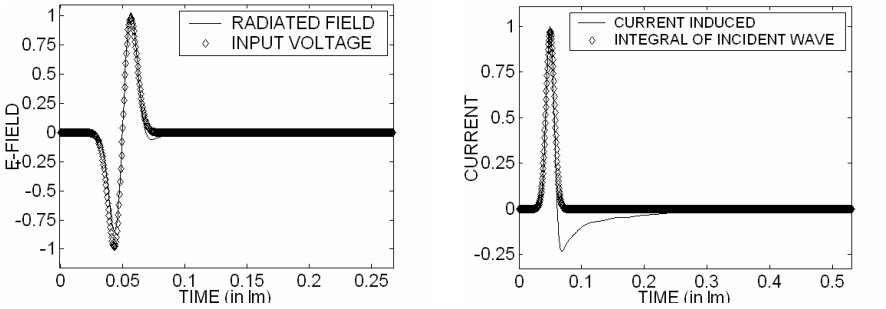


**Figure 13.** Radiated field for an ultra-wideband bicone.

where $C(a,x)$ and $S(a,x)$ are the generalized cosine and sine integrals:

$$C(a,x) = \int_0^x \frac{1-\cos W}{W} du \qquad S(a,x) = \int_0^x \frac{\sin W}{W} du \tag{5}$$

with

$$W = (u^2 + a^2)^{1/2} \tag{6}$$

So the continuously varying resistive profile can be defined as

$$z^i(z) = r^i(z) - j/\omega\, c^i(z) \;=\; \frac{\zeta_0 \psi}{2\pi} \frac{1}{h-|z|} \;=\; \frac{60\psi}{h-|z|} \tag{7}$$

In this formula the frequency dependence appears only in the form of a logarithm for small values of $kh$, so the antenna shows very broad frequency characteristics. The reactive part of the impedance is very small compared to the resistive part, so we do not need to implement the capacitive profile in this case. The value of $\psi$ at the frequency for which the bicone is a half-wavelength long is calculated and the effective radius for the load calculation in (4) is taken to be one-hundredth of the length of the bicone to meet the specification for a thin antenna. The antenna has been divided into lateral regions along its length and distributed loading is applied on each region by calculating the resistivity at the midpoint of that region. If the number of sections is sufficiently large, then the step-functional variation of the resistance will bear a close resemblance to the continuously varying resistive profile (Figure 12). The radiated field for this non-reflecting antenna nearly coincides with the input voltage (Figure 13(a)), which verifies that the reflectionless bicone behaves like an infinitely long dipole. If the antenna is used as a receiver, the received current at the feed point of the antenna deviates slightly from the integral of the input voltage (Figure 13(b)). This discrepancy is due to the absence of any dc current on the structure. This methodology illustrates the design of a angle-specific ultra-wideband antenna using bicone structures.

## 5. CONCLUSION

The spherically capped bicone antenna has been extensively studied in this paper. The antenna is considered with equal cone angles and with unequal cone angles. An investigation of the radiation pattern of the antenna shows that for $ka \ll 1$ the radiation pattern can be approximated by $\sin\theta$ whereas for $ka \gg 1$ the pattern lies within an angular area determined by the cone angles of the antenna. As an

example we can limit the radiation energy in the upper half of the $E$-plane within an angular region of 36.9° by choosing $\psi_1 = 53.1°$ and $\psi_2 = 90°$.

The transient response of the antenna has also been investigated for both radiation and reception for different sets of cone angles. Observation of the wave shapes from the antennas give important information about their transmitting and receiving properties and relationships can be obtained between the input and output wave shapes. Moreover it is observed that when $ka \ll 1$ the transient fields and currents are not affected by the change in the cone angles. But for $ka \gg 1$ there are reflections due to the finite nature of the antenna and these reflections change slightly with changes in the cone angle values.

The bicone antenna can be designed to have ultra-wideband behavior by using a spherical cap and by applying resistive loading on the structure. This antenna radiates most of the energy in the direction where the pulse is most similar to the exciting waveform. This property is very critical in the operation of ultra-wideband structures. Thus whether the need is for a wideband antenna with dipole-like isotropic patterns or for an ultra-wideband antenna with radiation constrained within a particular angular area, one can design it with a spherically capped bicone antenna as illustrated in this paper.

## REFERENCES

1. Schelkunoff, S. A., *Electromagnetic Waves*, Vol. 9, Van Nostrand, New York, 1943.
2. Smith, P. D. P., "The conical dipole of wide-angle," *Journal of Applied Physics*, Vol. 19, 11–23, 1948.
3. Papas, C. H. and R. W. P. King, "Input impedance of wide-angle conical antennas fed by a coaxial line," *Proceedings IRE*, Vol. 37, 1269–1271, 1949.
4. Papas, C. H. and R. W. P. King, "Radiations from wide-angle conical antenna fed by a coaxial line," *Proceeding IRE*, Vol. 39, 49–51, 1951.
5. Sandler, S. S. and R. P. W. King, "Compact conical antenna for wide-band coverage," *IEEE Transactions on Antenna and Propagation*, Vol. 42, 436–439, Mar. 1994.
6. Samaddar, S. N. and E. L. Mokole, "Biconical antenna with unequal cone angles," *IEEE Transactions on Antenna and Propagation*, Vol. 46, No. 2, 181–193, 1998.
7. Kolundzija, B. M., J. S. Ognjanovic, and T. K. Sarkar, *WIPL-D:*

*Software for Electromagnetic Analysis of Composite Wire, Plate and Dielectric Structures*, Artech House, 1995.

8. Ghosh, D., A. De, M. C. Taylor, T. K. Sarkar, M. C. Wicks, and E. Mokole, "Transmission and reception by ultra wideband (UWB) antennas," *IEEE Antenna and Propagation Magazine*, Vol. 48, No. 5, 66–99, Oct. 2006.
9. Sarkar, T. K., M. C. Wicks, M. Salazar-Palma, and R. J. Bonneau, *Smart Antennas*, Wiley-IEEE Press, Apr. 22, 2003.
10. Harrison, C. W. and R. W. P. King, "On the transient response of an infinite cylindrical antenna," *IEEE Transactions on Antenna and Propagation*, 301–302, 1967.
11. Kanda, M., "Time domain sensors and radiators," *Time Domain Measurements in Electromagnetics*, E. K. Miller (ed.), Vol. 5, Van Nostrand Reinhold, New York, 1986.
12. Chisholm, W. A. and W. Janischewskyj, "Lightning surge response of ground electrodes," *IEEE Trans. on Power Delivery*, Vol. 4, No. 2, 1329–1337, Apr. 1989.
13. Baba, Y. and V. A. Rakov, "On the interpretation of ground reflections observed in small-scale experiments simulating lightning strikes to towers," *IEEE Trans. on EMC*, Vol. 47, No. 3, 533–542, Aug. 2005.